WL-TR-93-1135

DIRECT-SEQUENCE SPREAD-SPECTRUM PERFORMANCE IN A MULTIPATH FADING ENVIRONMENT

TERRY D. NEBERGALL

COMMUNICATIONS TECHNOLOGY SECTION
NAVIGATION & INFORMATION TRANSMISSION BRANCH
SYSTEM AVIONICS DIVISION

SEPTEMBER 1993

FINAL REPORT FOR PERIOD 6 JANUARY 1993 - 24 AUGUST 1993

AVIONICS DIRECTORATE
WRIGHT LABORATORY
AIR FORCE MATERIEL COMMAND
WRIGHT PATTERSON AFB OH 45433-7409

NOTICE

WHEN GOVERNMENT DRAWINGS, SPECIFICATIONS, OR OTHER DATA ARE USED FOR ANY PURPOSE OTHER THAN IN CONNECTION WITH A DEFINITELY GOVERNMENT-RELATED PROCUREMENT, THE UNITED STATED GOVERNMENT INCURS NO RESPONSIBILITY OR ANY OBLIGATION WHATSOEVER. THE FACT THAT THE GOVERNMENT MAY HAVE FORMULATED OR IN ANY WAY SUPPLIED THE SAID DRAWINGS, SPECIFICATIONS, OR OTHER DATA, IS NOT TO BE REGARDED BY IMPLICATIONS, OR OTHERWISE IN ANY MANNER CONSTRUED, AS LICENSING THE HOLDER, OR ANY OTHER PERSON OR CORPORATION; OR AS CONVEYING ANY RIGHTS OR PERMISSION TO MANUFACTURE, USE, OR SELL ANY PATENTED INVENTION THAT MAY IN ANY WAY BE RELATED THERETO.

THIS TECHNICAL REPORT HAS BEEN REVIEWED AND IS APPROVED FOR PUBLICATION.

Terry D. Nebergall

TERRY NEBERGALL
Project Engineer

Franklin Hutson

FRANKLIN T. HUTSON, Chief
Communications Technology Section
System Avionics Division

Charles H Krueger

CHARLES H. KRUEGER, Chief
System Avionics Division
Avionics Directorate

IF YOUR ADDRESS HAS CHANGED, IF YOU WISH TO BE REMOVED FROM OUR MAILING LIST, OR IF THE ADDRESSEE IS NO LONGER EMPLOYED BY YOUR ORGANIZATION PLEASE NOTIFY WL/AAAI BLDG 635, 2185 AVIONICS CIRCLE, WRIGHT-PATTERSON AFB OH 45433-7301 TO HELP MAINTAIN A CURRENT MAILING LIST.

COPIES OF THIS REPORT SHOULD NOT BE RETURNED UNLESS RETURN IS REQUIRED BY SECURITY CONSIDERATIONS, CONTRACTUAL OBLIGATIONS, OR NOTICE ON A SPECIFIC DOCUMENT.

REPORT DOCUMENTATION PAGE

Form Approved
OMB No. 0704-0188

1. AGENCY USE ONLY *(Leave blank)*	2. REPORT DATE	3. REPORT TYPE AND DATES COVERED
	SEPTEMBER 1993	FINAL 6 Jan 93 - 24 Aug 93

4. TITLE AND SUBTITLE

Direct-Sequence Spread-Spectrum Performance in a Multipath Fading Environment

5. FUNDING NUMBERS

PE 88751
PR 9994
TA 00
WU 00

6. AUTHOR(S)

Terry D. Nebergall

7. PERFORMING ORGANIZATION NAME(S) AND ADDRESS(ES)

Avionics Directorate
Wright Laboratory
Air Force Materiel Command
Wright Patterson AFB OH 45433-7409

8. PERFORMING ORGANIZATION REPORT NUMBER

WL-TR-93-1135

9. SPONSORING / MONITORING AGENCY NAME(S) AND ADDRESS(ES)

Avionics Directorate
Wright Laboratory
Air Force Materiel Command
Wright Patterson AFB OH 45433-7409

10. SPONSORING / MONITORING AGENCY REPORT NUMBER

WL-TR-93-1135

11. SUPPLEMENTARY NOTES

Research performed at Communications & Signal Processing Laboratory, Department of Electrical Engineering and Computer Science, University of Michigan.

12a. DISTRIBUTION / AVAILABILITY STATEMENT

Approved for public release; distribution is unlimited.

12b. DISTRIBUTION CODE

13. ABSTRACT *(Maximum 200 words)*

The performance of coherent direct-sequence spread-spectrum communication systems with specular multipath fading is analyzed in terms of average probability of error. Approximations to such are based on the characteristic-function method. The probability mass function of the correlation receiver output is also derived with this approach. Numerical results are presented for various multipath environments with deterministic gain coefficients and channel coding applications.

14. SUBJECT TERMS

Spread-spectrum communications, multipath fading

15. NUMBER OF PAGES

54

16. PRICE CODE

17. SECURITY CLASSIFICATION OF REPORT	18. SECURITY CLASSIFICATION OF THIS PAGE	19. SECURITY CLASSIFICATION OF ABSTRACT	20. LIMITATION OF ABSTRACT
UNCLASSIFIED	UNCLASSIFIED	UNCLASSIFIED	UL

Acknowledgements

This thesis is written in partial fulfillment of the master's degree requirements in Electrical Engineering: Systems at The University of Michigan. The author would like to acknowledge the following for their contributions to this entire effort:

The U.S. Air Force, and, in particular, the Palace Knight Program for financial support throughout the master's program; specifically, my supervisor, Franklin T. Hutson, and mentor, Lawrence L. Gutman, both at Wright-Patterson AFB, for their technical advice.

My research advisor, Dr. Wayne E. Stark, for invaluable guidance throughout this project; in addition to my advisor, Dr. David L. Neuhoff and Dr. Kim A. Winick for their service on the thesis committee.

Table of Contents

List of Figures

1. Introduction

This thesis examines the performance of coherent phase-shift-keyed (PSK) direct-sequence spread-spectrum (DS/SS) communications in a specular multipath fading environment. In a previous discussion of this particular topic [1], the authors derived an expression for the average probability of error of a correlation receiver, based on the characteristic-function of the multipath interference, given an arbitrary number of paths with both deterministic or random gain coefficients. The channel model considered here is a direct extension of that presented in [1] with some important constraints and modifications. First, there always exists a nonfaded component in the zeroth path signal, i.e., the direct path plus multipath interference with relatively small delay in comparison to the direct path. Second, the range of the path delays is restricted such that intersymbol interference is due to the same pair of adjacent data bits for each of the reflected paths (case(i) in [1]). Third, for the sake of brevity, only deterministic gain coefficients are considered. Finally, the assumption that the path delay must be at least one chip period is removed and consideration is given to delays less than a chip.

As in [1], the average probability of error is approximated using the characteristic-function method. Specifically, the characteristic function of the multipath interference is numerically integrated using Simpson's method. This technique is extended also to compute the probability mass function of the receiver output.

The thesis is presented in the following fashion. Section 2 discusses the system and channel models. Section 3 provides a derivational analysis of the average probability of error for any desired range of path delays within model constraints. In Section 4, an analysis is provided for the performance of channel coding applications. Then, the models are numerically evaluated for the PSK DS/SS system in Section 5. Finally, the conclusions of these results are presented in Section 6. Following the text are two appendices. Appendix A links the characteristic-function method to an expression for the average probability of error. Appendix B contains the computer code used to produce the numerical results.

2. System and Channel Models

Transmitter

As presented in [1], a channel user starts with a data signal $b(t)$, a sequence of rectangular pulses, each of duration T , where the l-th pulse has amplitude b_l for $lT \leq t < (l+1)T$. The data (b_l) is viewed as a sequence of mutually independent random variables, each with equal probability of being +1 or -1. The signal is then spread by the waveform $x(t)$, given by

$$x(t) = x_i \upsilon(t - iT_c), \quad iT_c \leq t < (i+1)T_c \tag{1}$$

where x_i is the binary signature sequence and $\upsilon(s)$ is a rectangular chip waveform satisfying $\upsilon(s) = 1$ for $0 \leq s < T_c$ and $\upsilon(s) = 0$ otherwise [2]. T_c represents the chip duration for the transmitted signal. The processing gain N is defined as the ratio between the period of the data signal and the chipping period: i.e., $N = T/T_c$. Thus, the signature sequence (x_i) has a period of N also. Considering the transmitter power P and the phase angle of the PSK modulator θ, the created spread-spectrum signal $u(t)$ can be expressed as

$$u(t) = \sqrt{2P} b(t) x(t) \exp(j\theta). \tag{2}$$

Thus, with carrier frequency f_c , the transmitted signal for a PSK DS/SS system is given by

$$s(t) = Re[u(t) \exp(j2\pi f_c t)]. \tag{3}$$

Channel

The output signal $y(t)$ produced by the specular multipath channel consists of one direct path and L delayed paths and may be modeled as the sum of attenuated, phase-shifted, and delayed versions of the input signal $s(t)$. Thus, as in [1], it may be expressed as

$$y(t) = \sum_{n=0}^{L} Re\{g_n u(t-\tau_n)\exp[j2\pi f_c(t-\tau_n)]\} \tag{4}$$

where the complex gain coefficients g_n are given as

$$g_0 = \beta + \gamma_0 A_0 \exp(j\theta_0) \quad \text{and} \quad g_n = \gamma_n A_n \exp(j\theta_n), \quad 1 \le n \le L \tag{5}$$

for the nth delayed path. Here, $\gamma_n A_n$ and θ_n represent the attenuation and phase shift incurred from the reflection of the delayed paths, respectively, while τ_n is the nth path delay relative to the zeroth, or direct path, assuming that $\tau_0 = 0$. The parameter β signifies the gain coefficient for the nonfaded component of the direct path. Throughout the analysis, it is assumed that $\beta = 1$ and the random variables A_n are normalized to have second-order moments equal to 1. Also, γ_n^2 may be interpreted as the relative power of the nth delayed path as compared to the nonfaded component of the direct path.

As previously mentioned, the zeroth channel consists of a direct path plus the combination of all multipath interference with small relative delays in comparison. The nth component channel ($n > 0$) then represents multipath interference combinations with relative delay of approximately

τ_n. The variables A_n, θ_n, and τ_n are modeled as mutually independent random vectors with mutually independent components as well. That is, $\mathbf{A} = (A_1, A_2, \ldots, A_L)$, $\theta = (\theta_1, \theta_2, \ldots, \theta_L)$, and $\tau = (\tau_1, \tau_2, \ldots, \tau_L)$. It is also assumed that these quantities are independent of A_0 and θ_0.

In general, the range of the path delays is $0 < \tau_n < T$. To allow resolvable demodulation of the transmitted signal, this range is normally limited such that $T_c \leq \tau_n \leq T - T_c$. That is, the delays are at least one chipping period away from zero, to provide necessary receiver rejection of the delayed paths, and at least one chipping period away from T, so that the receiver will not demodulate the delayed paths as direct paths with one-period delay. However, for analytical purposes, this paper considers situations in which $0 \leq \tau_n \leq T - T_c$; the upper limit is preserved to model practical applications.

Receiver

The output of the channel $y(t)$ is combined with additive white Gaussian noise $n(t) \sim \mathcal{N}\left(0, \frac{N_0}{2}\right)$, producing the received signal $r(t)$. The receiver, in turn, correlates this signal with $\sqrt{2/T}x(t)\cos(2\pi f_c t)$ and integrates from 0 to T. Thus, the receiver output becomes

$$Z = \sqrt{\frac{2}{T}} \int_0^T r(t)x(t)\cos(2\pi f_c t)dt. \tag{6}$$

Making the necessary substitutions, (6) becomes

$$Z = \sqrt{\frac{2}{T}}\left\{\eta_0 + \sqrt{2P}\left(\int_0^T b(t)x^2(t)[\beta\cos(2\pi f_c t) + \gamma_0 A_0\cos(2\pi f_c t + \theta_0)]\cos(2\pi f_c t)dt\right.\right.$$
$$\left.\left. + \sum_{n=1}^{L}\int_0^T \gamma_n A_n b(t-\tau_n)x(t-\tau_n)x(t)\cos[2\pi f_c(t-\tau_n)+\theta_n]\cos(2\pi f_c t)dt\right)\right\}$$

where $\eta_0 \sim N\left(0, \frac{N_0 T}{4}\right)$. Because f_c is much larger than $1/T$ in practical systems, the double-frequency terms above may be ignored. Thus, the integrated output becomes

$$Z = \sqrt{\frac{2}{T}}\left\{\eta_0 + \sqrt{\frac{P}{2}}\left[b_0\left(\beta + \gamma_0 A_0\cos(\theta_0)\right)\int_0^T dt\right.\right.$$
$$\left.\left. + \sum_{n=1}^{L}\int_0^T \gamma_n A_n b(t-\tau_n)x(t-\tau_n)x(t)\cos(\phi_n)dt\right]\right\} \qquad (7)$$

where $\phi_n = \theta_n - 2\pi f_c\tau_n$. Both θ_n and θ_0 are assumed to be uniformly distributed in $[0, 2\pi]$. Similarly, because of the size of f_c in comparison to τ_n, the modulo-2π form for $\phi_n \sim U[0, 2\pi]$. Defining the multipath interference component for the zeroth path $F_0 = A_0 b_0\cos(\theta_0)$ and splitting the range of the integrand into the ranges $[0, \tau_n]$ and $[\tau_n, T]$, (7) becomes

$$Z = \sqrt{\frac{2}{T}}\left\{\eta_0 + \sqrt{\frac{P}{2}}\left[(\beta b_0 + \gamma_0 F_0)T + \sum_{n=1}^{L}\gamma_n A_n\cos(\phi_n)\left(\int_0^{\tau_n} b(t-\tau_n)x(t-\tau_n)x(t)dt\right.\right.\right.$$
$$\left.\left.\left. + \int_{\tau_n}^{T} b(t-\tau_n)x(t-\tau_n)x(t)dt\right)\right]\right\}.$$

From [3], the continuous partial autocorrelation functions of $x(t)$ are defined by

$$R_x(\tau_n) = \int_0^{\tau_n} x(t-\tau_n)x(t)dt. \quad 0 \le \tau_n \le T \quad \text{and} \quad \hat{R}_x(\tau_n) = R_x(T-\tau_n).$$

Thus, making these substitutions,

$$Z = \sqrt{\frac{2}{T}}\left\{\eta_0 + \sqrt{\frac{P}{2}}\left[(\beta b_0 + \gamma_0 F_0)T + \sum_{n=1}^{L}\gamma_n A_n \cos(\phi_n)\left(b_{-1}R_x(\tau_n) + b_0\hat{R}_x(\tau_n)\right)\right]\right\}. \quad (8)$$

The L other multipath interference components are given by

$$F_n = T^{-1}A_n[b_{-1}R_x(\tau_n) + b_0\hat{R}_x(\tau_n)]\cos(\phi_n). \quad (9)$$

Thus, it follows from (8),

$$Z = \sqrt{\frac{2}{T}}\left\{\eta_0 + \sqrt{\frac{P}{2}}\left[(\beta b_0 + \gamma_0 F_0)T + \sum_{n=1}^{L}\gamma_n F_n T\right]\right\}.$$

Finally, defining $E_b = PT$ as the energy per information bit of the transmitted signal, the integrated output reduces to

$$Z = \eta_0' + \sqrt{E_b}\left(\beta b_0 + \sum_{n=0}^{L}\gamma_n F_n\right) \quad (10)$$

where $\eta_0' \sim N(0, \frac{N_0}{2})$.

3. Average Probability of Error

The method applied in evaluating the average probability of error for the DS/SS system is the characteristic-function method, as employed in [1]. Here, the approximation is based on the integration of the characteristic-functions of the noise and multipath interference components of the correlated receiver. The analysis which follows considers deterministic gain coefficients g_n.

The gain coefficients are normalized such that $\beta = 1$ and A_n does actually equal 1 for $0 \leq n \leq L$. From (10), define the following:

$$\eta = \eta_0'/\sqrt{E_b} \tag{11}$$

$$I = \sum_{n=0}^{L} \gamma_n F_n. \tag{12}$$

This, in turn, implies that

$$Z = \sqrt{E_b}(\eta + b_0 + I). \tag{13}$$

Since the decision of the receiver is based on comparing the output Z with a zero threshold, the average probability of error conditioned on b_0 is written as

$$\begin{aligned} \bar{P}_e &= \frac{1}{2}P(Z \leq 0|b_0 = +1) + \frac{1}{2}P(Z > 0|b_0 = -1) \\ &= \frac{1}{2}[P(\eta + I \leq -1) + P(\eta + I > 1)] \\ &= \frac{1}{2} - \frac{1}{2}P(-1 < \eta + I \leq 1). \end{aligned} \tag{14}$$

As demonstrated in Appendix A, this expression becomes

$$\bar{P}_e = Q(\sigma^{-1}) + \frac{1}{\pi}\int_0^\infty \mathrm{sinc}(u/\pi)\phi_\eta(u)[1-\phi_I(u)]du \tag{15}$$

where $Q(x) = \frac{1}{\sqrt{2\pi}}\int_x^\infty \exp(-t^2/2)dt$, $\sigma^2 = (2E_b/N_0)^{-1}$ is the variance of η. and ϕ_η and ϕ_I are the respective characteristic functions of η and I. Since η is a Gaussian random variable, its characteristic function is given by

$$\begin{aligned}\phi_\eta(u) &= \exp\left(ju\bar{\eta} - \frac{1}{2}u^2\sigma^2\right) \\ &= \exp\left(-\frac{1}{2}u^2\sigma^2\right)\end{aligned} \tag{16}$$

recalling that η is zero mean. The characteristic function of the interference sum I, can be expressed as the product

$$\phi_I = \tilde{\phi}_0(u)\tilde{\phi}(u) \tag{17}$$

where $\tilde{\phi}_0(u)$ represents the characteristic function of the direct-path faded component $\gamma_0 F_0$ and $\tilde{\phi}(u)$ denotes the characteristic function for the interference components $\sum_{n=1}^{L}\gamma_n F_n$. For the direct-path,

$$\begin{aligned}\tilde{\phi}_0(u) &= E[\exp(ju\gamma_0 F_0)] \\ &= \frac{1}{2\pi}\int_0^{2\pi}\exp(ju\gamma_0 b_0\cos\theta)d\theta \\ &= \frac{1}{2\pi}\int_0^{2\pi}\cos(u\gamma_0 b_0\cos\theta)d\theta \\ &= \frac{2}{\pi}\int_0^{\pi/2}\cos(\gamma_0 u\cos\theta)d\theta\end{aligned} \tag{18}$$

where the sine component of the complex exponential integrates to zero. From (10), there are two cases to consider in evaluating $\tilde{\phi}(u)$: $b_{-1} = b_0$ and

$b_{-1} \neq b_0$, both of which are equally likely to occur. Also, as opposed to the path delay restriction of [1], τ is assumed to be uniformly distributed in $[M_1T_c, M_2T_c]$, where M_1 and M_2 are integers and $M_1 < M_2$. Thus,

$$\begin{aligned}
\tilde{\phi}(u) &= \frac{1}{2}E\left[\exp\left(ju\sum_{n=1}^{L}\gamma_n F_n(b_{-1}=b_0)\right)\right] + \frac{1}{2}E\left[\exp\left(ju\sum_{n=1}^{L}\gamma_n F_n(b_{-1}\neq b_0)\right)\right] \\
&= \frac{1}{2}\prod_{n=1}^{L}E\left[\exp\left(ju\gamma_n F_n(b_{-1}=b_0)\right)\right] + \frac{1}{2}\prod_{n=1}^{L}E\left[\exp\left(ju\gamma_n F_n(b_{-1}\neq b_0)\right)\right] \\
&= \frac{1}{2}\prod_{n=1}^{L}M\int_0^{2\pi}\int_{M_1T_c}^{M_2T_c}\exp\left[ju\gamma_n\left(R_x(\tau)+\hat{R}_x(\tau)\right)\frac{\cos\phi}{T}\right]d\tau d\phi \\
&\quad + \frac{1}{2}\prod_{n=1}^{L}M\int_0^{2\pi}\int_{M_1T_c}^{M_2T_c}\exp\left[ju\gamma_n\left(-R_x(\tau)+\hat{R}_x(\tau)\right)\frac{\cos\phi}{T}\right]d\tau d\phi \qquad (19)
\end{aligned}$$

where the constant M is defined by

$$M = \frac{1}{2\pi(M_2-M_1)T_c}.$$

Because I has symmetric distribution, the characteristic functions $\tilde{\phi}_0$ and $\tilde{\phi}$ must be real and even; i.e., $\tilde{\phi}(u) = \tilde{\phi}(-u)$. The autocorrelation functions R_x and $\hat{R}_x$ are defined in [3] in terms of the discrete aperiodic autocorrelation function C_x of the signature sequence (x_i), and the chip waveform partial autocorrelation functions R_ψ and $\hat{R}_\psi$. That is,

$$R_x(\tau) = C_x(N-l)\hat{R}_\psi(\tau - lT_c) + C_x(N-l-1)R_\psi(\tau - lT_c)$$

and

$$\hat{R}_x(\tau) = C_x(l)\hat{R}_\psi(\tau - lT_c) + C_x(l+1)R_\psi(\tau - lT_c)$$

where l denotes the integer part of τ/T_c, $\hat{R}_\psi(s) = \int_s^{T_c} \psi(t)\psi(t-s)dt$, and $R_\psi(s) = \int_s^{T_c} \psi(t)\psi(t+T_c-s)dt$ for $0 \le s \le T_c$. Thus, (19) becomes

$$\begin{aligned}
\tilde{\phi}(u) &= \frac{1}{2}\prod_{n=1}^{L} M \int_0^{2\pi}\int_{M_1T_c}^{M_2T_c} \cos\{u\gamma_n[(C_x(N-l-1)+C_x(l+1))R_\psi(\tau-lT_c) \\
&+ (C_x(N-l)+C_x(l))\hat{R}_\psi(\tau-lT_c)]\frac{\cos\phi}{T}\Big\} d\tau d\phi \\
&+ \frac{1}{2}\prod_{n=1}^{L} M \int_0^{2\pi}\int_{M_1T_c}^{M_2T_c} \cos\{u\gamma_n[(-C_x(N-l-1)+C_x(l+1))R_\psi(\tau-lT_c) \\
&+ (-C_x(N-l)+C_x(l))\hat{R}_\psi(\tau-lT_c)]\frac{\cos\phi}{T}\Big\} d\tau d\phi.
\end{aligned}$$

From [4], the periodic (even) and odd autocorrelation functions for the chip waveform are respectively defined by

$$\theta_x(l) = C_x(l) + C_x(l-N), \quad 0 \le l \le N-1$$

and

$$\hat{\theta}_x(l) = C_x(l) - C_x(l-N), \quad 0 \le l \le N-1.$$

Making these substitutions,

$$\begin{aligned}
\tilde{\phi}(u) &= \frac{1}{2}\prod_{n=1}^{L} M \int_0^{2\pi}\int_{M_1T_c}^{M_2T_c} \cos\left\{u\gamma_n\left[\theta_x(l+1)R_\psi(\tau-lT_c)+\theta_x(l)\hat{R}_\psi(\tau-lT_c)\right]\frac{\cos\phi}{T}\right\} d\tau d\phi \\
&+ \frac{1}{2}\prod_{n=1}^{L} M \int_0^{2\pi}\int_{M_1T_c}^{M_2T_c} \cos\left\{u\gamma_n\left[\hat{\theta}_x(l+1)R_\psi(\tau-lT_c)+\hat{\theta}_x(l)\hat{R}_\psi(\tau-lT_c)\right]\frac{\cos\phi}{T}\right\} d\tau d\phi
\end{aligned}$$

for $0 \le l \le N-2$. Considering the variable substitution $s = \tau - lT_c$,

$$
\begin{aligned}
\tilde{\phi}(u) &= \frac{1}{2}\prod_{n=1}^{L} M \int_0^{2\pi}\sum_{l=M_1}^{M_2-1}\int_0^{T_c}\cos\left\{u\gamma_n\left[\theta_x(l+1)R_\psi(s)+\theta_x(l)\hat{R}_\psi(s)\right]\frac{\cos\phi}{T}\right\}dsd\phi \\
&+ \frac{1}{2}\prod_{n=1}^{L} M \int_0^{2\pi}\sum_{l=M_1}^{M_2-1}\int_0^{T_c}\cos\left\{u\gamma_n\left[\hat{\theta}_x(l+1)R_\psi(s)+\hat{\theta}_x(l)\hat{R}_\psi(s)\right]\frac{\cos\phi}{T}\right\}dsd\phi \\
&= \frac{1}{2}\prod_{n=1}^{L} 4M \sum_{l=M_1}^{M_2-1}\int_0^{\pi/2}\int_0^{T_c}\cos\left\{u\gamma_n\left[\theta_x(l+1)R_\psi(s)+\theta_x(l)\hat{R}_\psi(s)\right]\frac{\cos\phi}{T}\right\}dsd\phi \\
&+ \frac{1}{2}\prod_{n=1}^{L} 4M \sum_{l=M_1}^{M_2-1}\int_0^{\pi/2}\int_0^{T_c}\cos\left\{u\gamma_n\left[\hat{\theta}_x(l+1)R_\psi(s)+\hat{\theta}_x(l)\hat{R}_\psi(s)\right]\frac{\cos\phi}{T}\right\}dsd\phi \\
&= \frac{1}{2}\left\{\prod_{n=1}^{L}\left[\frac{1}{M_2-M_1}\sum_{l=M_1}^{M_2-1} f(\gamma_n u; l, \theta_x)\right] + \prod_{n=1}^{L}\left[\frac{1}{M_2-M_1}\sum_{l=M_1}^{M_2-1} f(\gamma_n u; l, \hat{\theta}_x)\right]\right\} \quad (20)
\end{aligned}
$$

where

$$
f(v; l, h) = \frac{2}{\pi T_c}\int_0^{\pi/2}\int_0^{T_c}\cos\left\{v\left[h(l+1)R_\psi(s)+h(l)\hat{R}_\psi(s)\right]\frac{\cos\phi}{T}\right\}dsd\phi. \quad (21)
$$

For the chip waveform described in (1), the partial autocorrelation functions become $R_\psi(s) = s$ and $\hat{R}_\psi(s) = T_c - s$, $0 \le s \le T_c$ [2]. So, for the BPSK system, the function in (21) becomes

$$
\begin{aligned}
f(v; l, h) &= \frac{2}{\pi T_c}\int_0^{\pi/2}\int_0^{T_c}\cos\left\{v\left[h(l+1)s + h(l)(T_c - s)\right]\frac{\cos\phi}{T}\right\}dsd\phi \\
&= \frac{2}{\pi T_c}\int_0^{\pi/2}\frac{\sin\left[vh(l+1)T_cT^{-1}\cos\phi\right] - \sin\left[vh(l)T_cT^{-1}\cos\phi\right]}{v\left[h(l+1)-h(l)\right]T^{-1}\cos\varphi}d\phi.
\end{aligned}
$$

Applying the trigonometric identity

$$
\sin(2A) - \sin(2B) = 2\sin(A-B)\cos(A+B),
$$

this expression reduces to

$$f(v;l,h) = \frac{2}{\pi}\int_0^{\pi/2} \frac{2\sin\left\{v\left[h(l+1)-h(l)\right]\frac{\cos\phi}{2N}\right\}\cos\left\{v\left[h(l+1)+h(l)\right]\frac{\cos\phi}{2N}\right\}}{v\left[h(l+1)-h(l)\right]\frac{\cos\phi}{N}} d\phi$$

$$= \frac{2}{\pi}\int_0^{\pi/2} \mathrm{sinc}\left\{v\left[h(l+1)-h(l)\right]\frac{\cos\phi}{2\pi N}\right\}\cos\left\{v\left[h(l+1)+h(l)\right]\frac{\cos\phi}{2N}\right\} d\phi \quad (22)$$

which is the form obtained in (14) of [2].

For comparative analysis, the Gaussian approximation of the probability of error is derived by applying the average signal-to-noise ratio at the receiver output when there is no power in the faded component of the zeroth path (i.e., $\gamma_0 = 0$). As in [3], SNR_0 is defined by

$$SNR_0 = E[Z|b_0=+1]\{\mathrm{Var}[Z|b_0=+1]\}^{-1/2}$$

$$= \sqrt{E_b}\left\{E\left[1+\sum_{n=1}^{L}\gamma_n F_n\right]\right\}\left\{\mathrm{Var}\left[\eta_0' + \sqrt{E_b}\left(1+\sum_{n=1}^{L}\gamma_n F_n\right)\right]\right\}^{-1/2}$$

$$= \sqrt{E_b}\left\{\mathrm{Var}(\eta_0') + E_b\mathrm{Var}\left[\sum_{n=1}^{L}\gamma_n F_n\right]\right\}^{-1/2} \quad (23)$$

Since $E\left[\sum_{n=1}^{L}\gamma_n F_n\right] = 0$, $\mathrm{Var}\left[\sum_{n=1}^{L}\gamma_n F_n\right] = \sum_{n=1}^{L}\gamma_n^2 E(F_n^2)$, where

$$E(F_n^2) = E\{T^{-2}[b_{-1}R_x(\tau_n) + \hat{R}_x(\tau_n)]^2\cos^2(\phi_n)\}$$

$$= \frac{1}{2}T^{-2}E\{[b_{-1}R_x(\tau_n) + \hat{R}_x(\tau_n)]^2\}$$

$$= \frac{1}{2}T^{-2}E[R_x^2(\tau_n) + \hat{R}_x^2(\tau_n)]$$

$$= \frac{1}{2}T^{-2}\frac{1}{M_2T_c - M_1T_c}\int_{M_1T_c}^{M_2T_c}[R_x^2(\tau) + \hat{R}_x^2(\tau)]d\tau.$$

Making this substitution, (23) becomes

$$
\begin{aligned}
SNR_0 &= \sqrt{E_b}\left\{\frac{N_0}{2} + E_b\,\frac{1}{2T^2T_c(M_2-M_1)}\sum_{n=1}^{L}\gamma_n^2\int_{M_1T_c}^{M_2T_c}[R_x^2(\tau)+\hat{R}_x^2(\tau)]d\tau\right\}^{-1/2} \\
&= \left\{\frac{N_0}{2E_b} + \frac{1}{2}\,\frac{1}{T^2T_c(M_2-M_1)}\sum_{n=1}^{L}\gamma_n^2\int_{M_1T_c}^{M_2T_c}[R_x^2(\tau)+\hat{R}_x^2(\tau)]d\tau\right\}^{-1/2} \\
&= \left\{\left(\frac{2E_b}{N_0}\right)^{-1} + \frac{1}{2}[T^2T_c(M_2-M_1)]^{-1}\sum_{n=1}^{L}\gamma_n^2\int_{M_1T_c}^{M_2T_c}[R_x^2(\tau)+\hat{R}_x^2(\tau)]d\tau\right\}^{-1/2}. \quad (24)
\end{aligned}
$$

Substituting the expressions for R_x and $\hat{R}_x$, the sum within the integral becomes

$$
\begin{aligned}
R_x^2(\tau)+\hat{R}_x^2(\tau) &= [C_x(N-l)\hat{R}_\psi(\tau-lT_c)+C_x(N-l-1)R_\psi(\tau-lT_c)]^2 \\
&\quad +[C_x(l)\hat{R}_\psi(\tau-lT_c)+C_x(l+1)R_\psi(\tau-lT_c)]^2 \\
&= \hat{R}_\psi^2(\tau-lT_c)[C_x^2(N-l)+C_x^2(l)] \\
&\quad +2\hat{R}_\psi(\tau-lT_c)R_\psi(\tau-lT_c)[C_x(N-l)C_x(N-l-1)+C_x(l)C_x(l+1)] \\
&\quad +R_\psi^2(\tau-lT_c)[C_x^2(N-l-1)+C_x^2(l+1)].
\end{aligned}
$$

Again, letting $s=\tau-lT_c$ and realizing the expressions for $R_\psi(s)$ and $\hat{R}_\psi(s)$,

$$
\int_{M_1T_c}^{M_2T_c}[R_x^2(\tau)+\hat{R}_x^2(\tau)]d\tau
$$

$$
\begin{aligned}
&= \sum_{l=M_1}^{M_2-1}\int_0^{T_c}\{(T_c-s)^2[C_x^2(N-l)+C_x^2(l)]+2(T_c-s)(s)[C_x(N-l)C_x(N-l-1) \\
&\quad +C_x(l)C_x(l+1)]+s^2[C_x^2(N-l-1)+C_x^2(l+1)]\} \\
&= \sum_{l=M_1}^{M_2-1}\left\{-[C_x^2(N-l)+C_x^2(l)]\frac{(T_c-s)^3}{3}\right. \\
&\quad \left.+2[C_x(N-l)C_x(N-l-1)+C_x(l)C_x(l+1)]\left(\frac{T_cs^2}{2}-\frac{s^3}{3}\right)\right.
\end{aligned}
$$

$$+ [C_x^2(N-l-1) + C_x^2(l+1)]\frac{s^3}{3}\Bigg\}\Bigg|_0^{T_c}$$

$$= \sum_{l=M_1}^{M_2-1}\left\{2\left(\frac{T_c^3}{6}\right)[C_x(N-l)C_x(N-l-1) + C_x(l)C_x(l+1)]\right.$$

$$\left. + \frac{T_c^3}{3}[C_x^2(N-l-1) + C_x^2(l+1) + C_x^2(N-l) + C_x^2(l)]\right\}.$$

Thus, the signal-to-noise ratio reduces to

$$SNR_0 = \left\{\left(\frac{2E_b}{N_0}\right)^{-1} + \frac{1}{2}[T^2(M_2T_c - M_1T_c)]^{-1}\sum_{n=1}^{L}\gamma_n^2\sum_{l=M_1}^{M_2-1}\frac{T_c^3}{3}[C_x(N-l)C_x(N-l-1)\right.$$

$$\left. + C_x(l)C_x(l+1) + C_x^2(N-l-1) + C_x^2(l+1) + C_x^2(N-l) + C_x^2(l)]\right\}^{-1/2}$$

$$= \left\{\left(\frac{2E_b}{N_0}\right)^{-1} + \frac{L\gamma_n^2}{6}\sum_{l=M_1}^{M_2-1}[C_x(N-l)C_x(N-l-1) + C_x(l)C_x(l+1)\right.$$

$$\left. + C_x^2(N-l-1) + C_x^2(l+1) + C_x^2(N-l) + C_x^2(l)]\frac{T_c^3}{(NT_c)^2(M_2T_c - M_1T_c)}\right\}^{-1/2}$$

$$= \left\{\left(\frac{2E_b}{N_0}\right)^{-1} + \frac{L\gamma_n^2}{6N^2(M_2-M_1)}\sum_{l=M_1}^{M_2-1}[C_x(N-l)C_x(N-l-1) + C_x(l)C_x(l+1)\right.$$

$$\left. + C_x^2(N-l-1) + C_x^2(l+1) + C_x^2(N-l) + C_x^2(l)]\right\}^{-1/2}. \qquad (25)$$

When consideration is given to the case $\gamma_0 \neq 0$, the Gaussian approximation to the probability of error must be conditioned on the phase shift θ_0, as seen in the expression for F_0. Thus, as in [1], the approximation becomes

$$P_G = \frac{1}{2\pi}\int_0^{2\pi} Q[SNR_0(1+\gamma_0\cos\theta)]d\theta. \qquad (26)$$

4. Coded Performance Analysis

The performance of the spread-spectrum system is enhanced with the addition of channel coding, as one may anticipate. Due to the hardware constraints for physical application of such systems, it becomes necessary to quantize the continuous receiver output Z in order to examine the effects of coding. We start by defining W as a quantization function of Z; that is,

$$W = w_j \quad \text{for} \quad a_j \leq Z < a_{j+1}, \quad j = 1, 2, ..., J$$

where $a_1 = -\infty$ and $a_J = +\infty$. Here, a_j represents the lower quantization threshold for quantization level j and we assume perfect interleaving. For coding with soft decisions there are many levels j, while with hard decisions, j is only as high as two. It follows from (13) then that the probability mass function (pmf) for W is given by

$$\begin{aligned} P\{W = w_j\} &= P(a_j \leq Z < a_{j+1}) \\ &= P[a_j \leq \sqrt{E}(\eta + b_0 + I) < a_{j+1}]. \end{aligned} \tag{27}$$

Here, E_b is replaced by E, the energy per code symbol; in general, for rate-r coding, $E = rE_b$. Letting ϕ represent the characteristic function for the sum $\eta + I$, and noting that ϕ is an even function,

$$P(a_j \leq Z < a_{j+1}|b_0) = \int_{\frac{a_j}{\sqrt{E}} - b_0}^{\frac{a_{j+1}}{\sqrt{E}} - b_0} \frac{1}{\pi} \int_0^\infty \phi(u) \cos(gu) du dg. \tag{28}$$

As shown in Appendix A, one may replace $\phi(u) = \phi_\eta(u)\phi_I(u)$ with $\phi_\eta(u) - \phi_\eta(u)[1-\phi_I(u)]$ to avoid subtracting numbers large relative to their difference.

Thus, (28) becomes

$$P(a_j \le Z < a_{j+1}|b_0) = \frac{1}{\pi}\int_0^\infty u^{-1}d(u)\phi_\eta(u)du - \frac{1}{\pi}\int_0^\infty u^{-1}d(u)\phi_\eta(u)[1-\phi_I(u)]du \quad (29)$$

where ϕ_η and ϕ_I are given in (16)-(20) and the function $d(u)$ is defined by

$$d(u) = \sin\left[\left(\frac{a_{j+1}}{\sqrt{E}} - b_0\right)u\right] - \sin\left[\left(\frac{a_j}{\sqrt{E}} - b_0\right)u\right].$$

For channel coding, an upper bound to the probability of error may be determined using D-parameter analysis. Denoting the conditional probability mass function by $p(w_j|b_0)$, the distance measure is approximated by

$$D = \sum_{j=1}^{J}\sqrt{p(w_j|+1)p(w_j|-1)} \quad (30)$$

for J quantization levels. The probability error bound is then expressed as a polynomial function of D. For example, for a channel with rate-1/2 convolutional code,

$$P_e \le 36D^{10} + 211D^{12} + 1404D^{14} + 11633D^{16} + 77433D^{18} + 502690D^{20} \quad (31)$$

while for convolutional coding with rate 1/3,

$$P_e \le 11D^{18} + 32D^{20} + 195D^{22} + 564D^{24} + 1473D^{26}, \quad (32)$$

where the weight enumerator polynomials are constructed from Tables I and II of [6].

5. Numerical Results

For all of the following examples, the signature sequences were generated from the method for auto-optimal (AO) / least-sidelobe-energy (LSE) maximal-length (m) sequences, as described in [4]. Specifically, the parameters listed in Figure A.1 [4] (or [5] when necessary) were applied to a linear feedback shift register to produce the desired binary chipping code (i.e., +1 and -1 values). These sequences were chosen for their structure simplicity and good correlation properties [4]. As in [1], it is assumed that the relative power in the nth path $\gamma_n^2 = \gamma^2$ for $1 \leq n \leq L$, but the faded component power in the zeroth path, γ_0^2, does not necessarily equal γ^2. In fact, for many instances γ_0^2 will assume a zero value (i.e., no faded component in the zeroth path). All of the numerical results were evaluated using the computer programs listed in Appendix B.

The first example considers the effect on the average probability of error, determined from the characteristic-function method (15), when the path delay is less than a chipping period. Figure 1 shows a comparison in error probability between two PSK DS/SS systems, each multipath channel with $L = 5$ reflected paths, individually having relative power $\gamma^2 = 0.4$, and $\gamma_0^2 = 0.1$. The signature sequence used is the $N = 31$ sequence taken from the first line of Figure A.1 [4]. In the first system, the path delay τ is uniformly distributed in $[T_c, T - T_c]$, while in the second, the delay ranges uniformly in $[0, T - T_c]$.

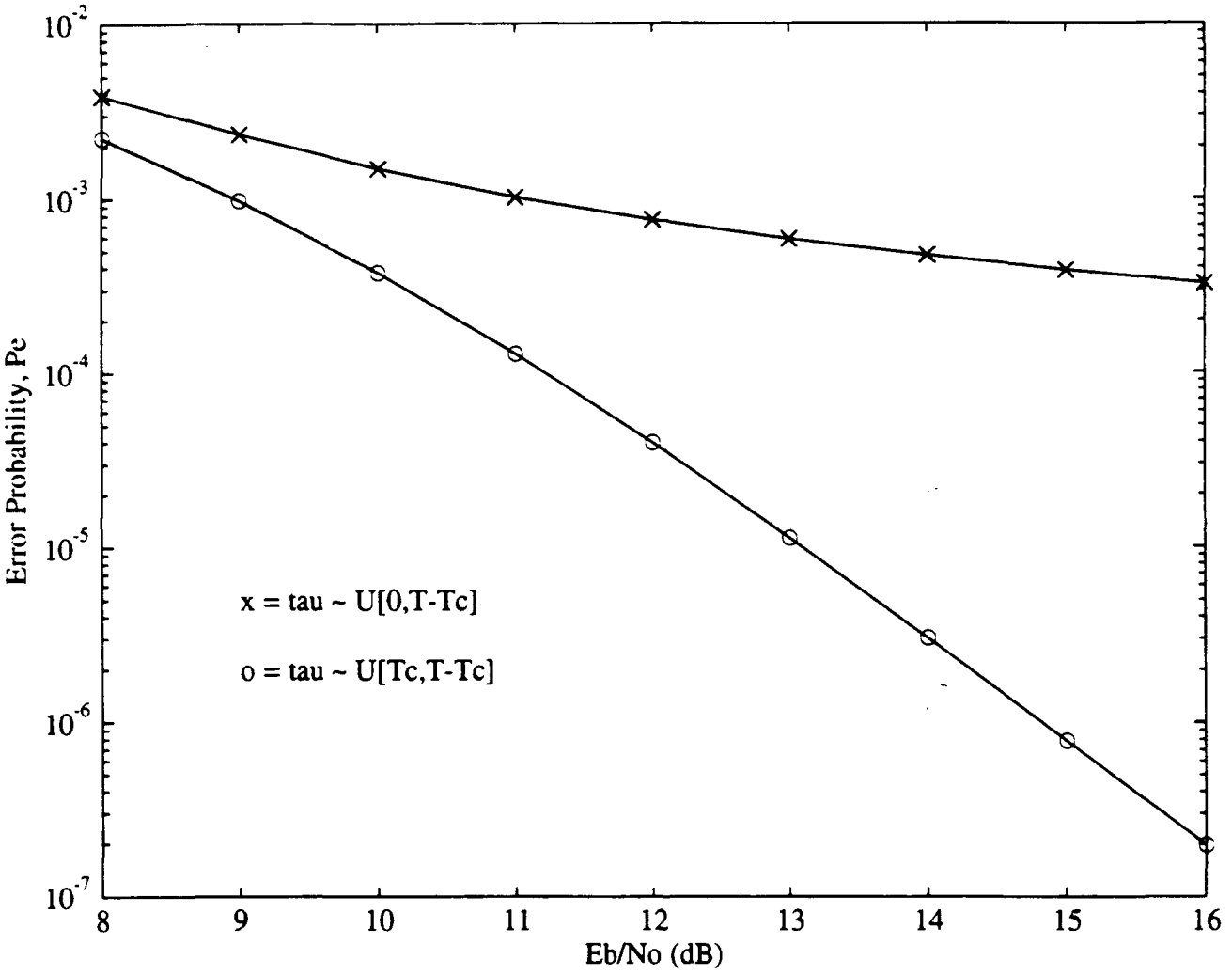

Figure 1: Probability of error for varied path delay uniformity ($N = 31, L = 5, \gamma^2 = 0.4, \gamma_0^2 = 0.1$).

According to the figure, the system performs well when the path delay is at least one chipping period: the probability of error quickly decreases for increasing E_b/N_0 values. However, when $\tau \sim U[0, T - T_c]$, the error probability decreases at a much slower rate and eventually levels off at about 10^{-4}. This demonstrates the fact that in the second system the multipath interference component arrives too close to the zeroth path signal. As a result, the receiver is unable to reject the delayed path effects.

The second example is a comparison between narrowband and broadband spread-spectrum systems. In the first case (narrowband), a signature sequence of length $N = 127$ is created using shift register polynomial parameter $\mathcal{H} = 301$ and initial register loading $\alpha_0 = 0010010$ [5]. The multipath channel has 5 delayed paths, each with $\tau \sim U[0, 10T_c]$. For the broadband case, a sequence of length $N = 1023$ is generated using $\mathcal{H} = 2201$ and $\alpha_0 = 0111011010$ [5]. Here, each of the 5 paths is uniformly distributed in $[0, 80T_c]$. This corresponds to the same delay spread if the data rate is as in the $N = 127$ case. In both cases, the faded component of the zeroth path is removed (i.e., $\gamma_0^2 = 0$), and each path has relative power $\gamma^2 = 0.4$. Figure 2 shows the probability of error for each application.

As one might expect, the broadband application outperforms the narrowband one for higher values of E_b/N_0. Clearly, as N increases, the chipping period T_c must decrease, assuming constant data pulse length T; thus, providing greater multipath rejection capability for the receiver and, hence, lower

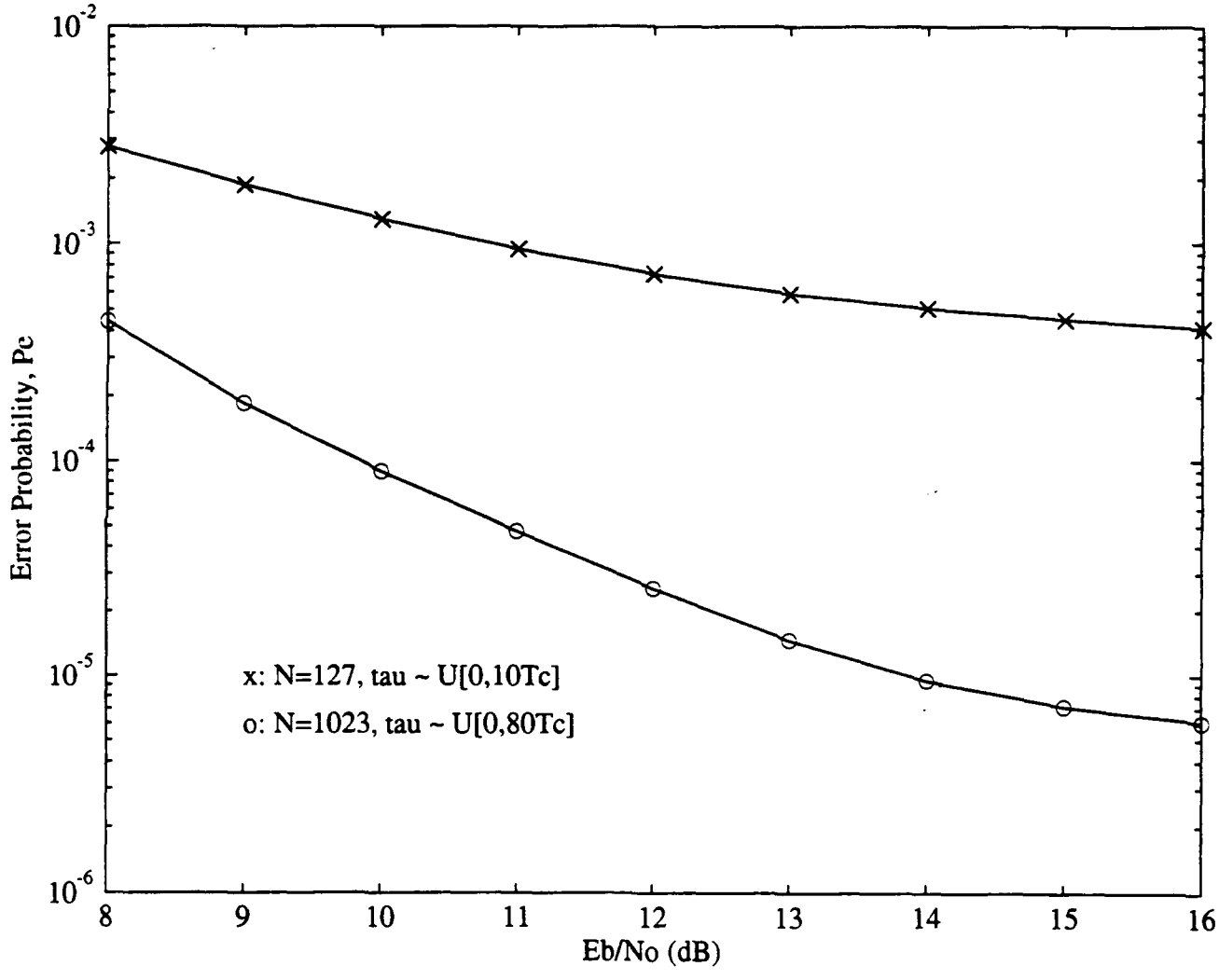

Figure 2: Probability of error for narrowband and broadband applications ($L = 5, \gamma^2 = 0.4, \gamma_0^2 = 0$).

error probability. However, such performance comes at the expense of increased bandwidth and system complexity (more shift registers are required for sequence generation).

In the next example, the average probability of error is analyzed for the two systems of Figure 2 as a function of the number of reflected, or delayed, paths L. For a fixed E_b/N_0 value of 10 dB, Figure 3 demonstrates that this measure of performance increases as more paths are added to the channel.

For the fourth example, the narrowband and broadband spread-spectrum systems are examined for a particular multipath environment. There are a total of $L = 12$ delayed paths, divided into four groups of three paths, each group with a particular relative power for the individual paths, and $\gamma_0^2 = 0$. For the narrowband ($N = 127$ chips/data bit), there are:

3 paths: $\tau \sim U[0, 4T_c]$, $\gamma^2 = 1$
3 paths: $\tau \sim U[24T_c, 28T_c]$, $\gamma^2 = 0.1$
3 paths: $\tau \sim U[48T_c, 52T_c]$, $\gamma^2 = 0.1$
3 paths: $\tau \sim U[96T_c, 100T_c]$, $\gamma^2 = 0.03$

For the broadband ($N = 1023$ chips/data bit), the length of each data pulse T is maintained from the narrowband case. Thus, the 12 paths for this system are divided as follows:

3 paths: $\tau \sim U[0, 33T_c]$, $\gamma^2 = 1$
3 paths: $\tau \sim U[194T_c, 226T_c]$, $\gamma^2 = 0.1$
3 paths: $\tau \sim U[387T_c, 419T_c]$, $\gamma^2 = 0.1$
3 paths: $\tau \sim U[774T_c, 806T_c]$, $\gamma^2 = 0.03$

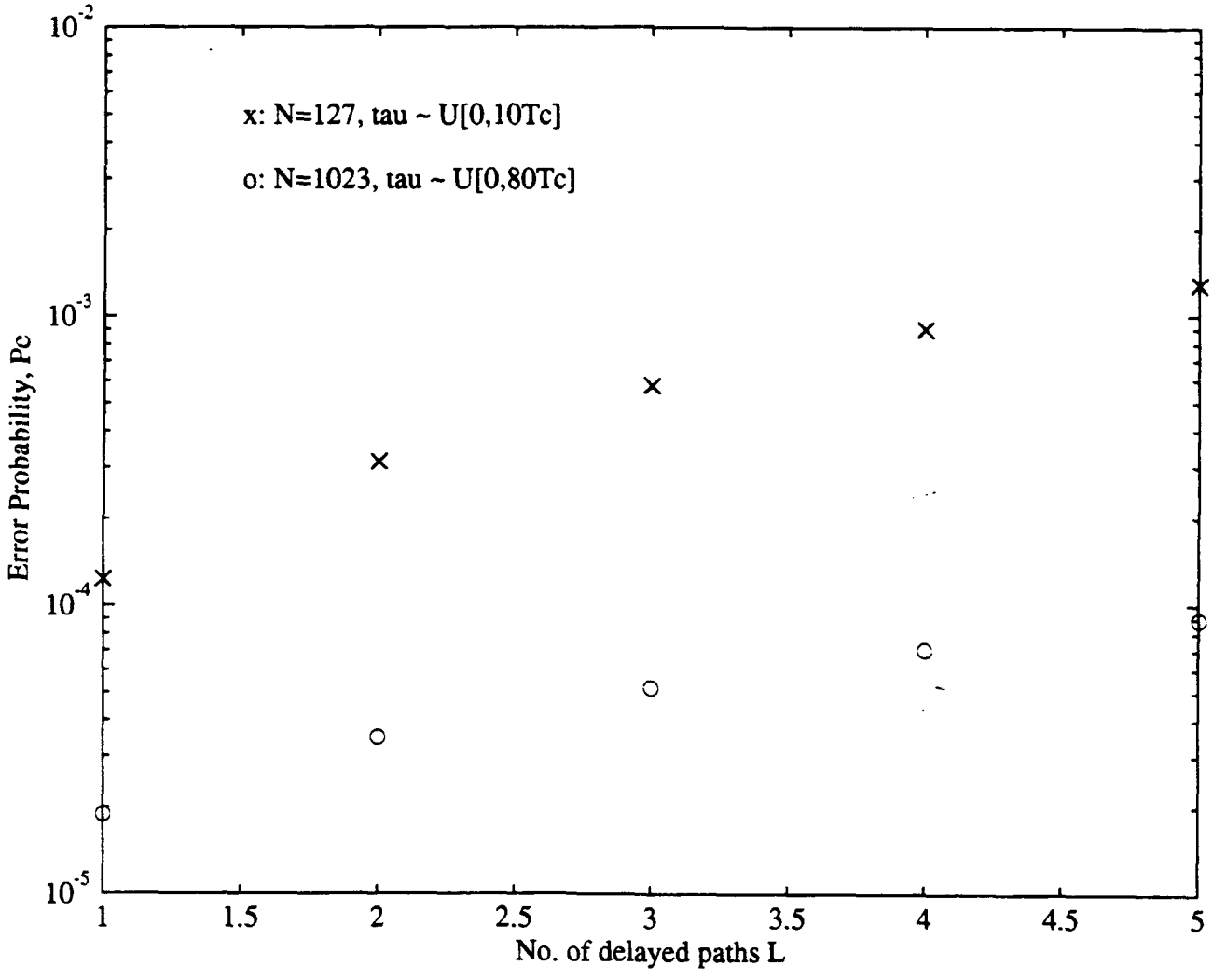

Figure 3: Probability of error for increasing number of delayed paths ($E_b/N_0 = 10$ dB, $\gamma^2 = 0.4, \gamma_0^2 = 0$).

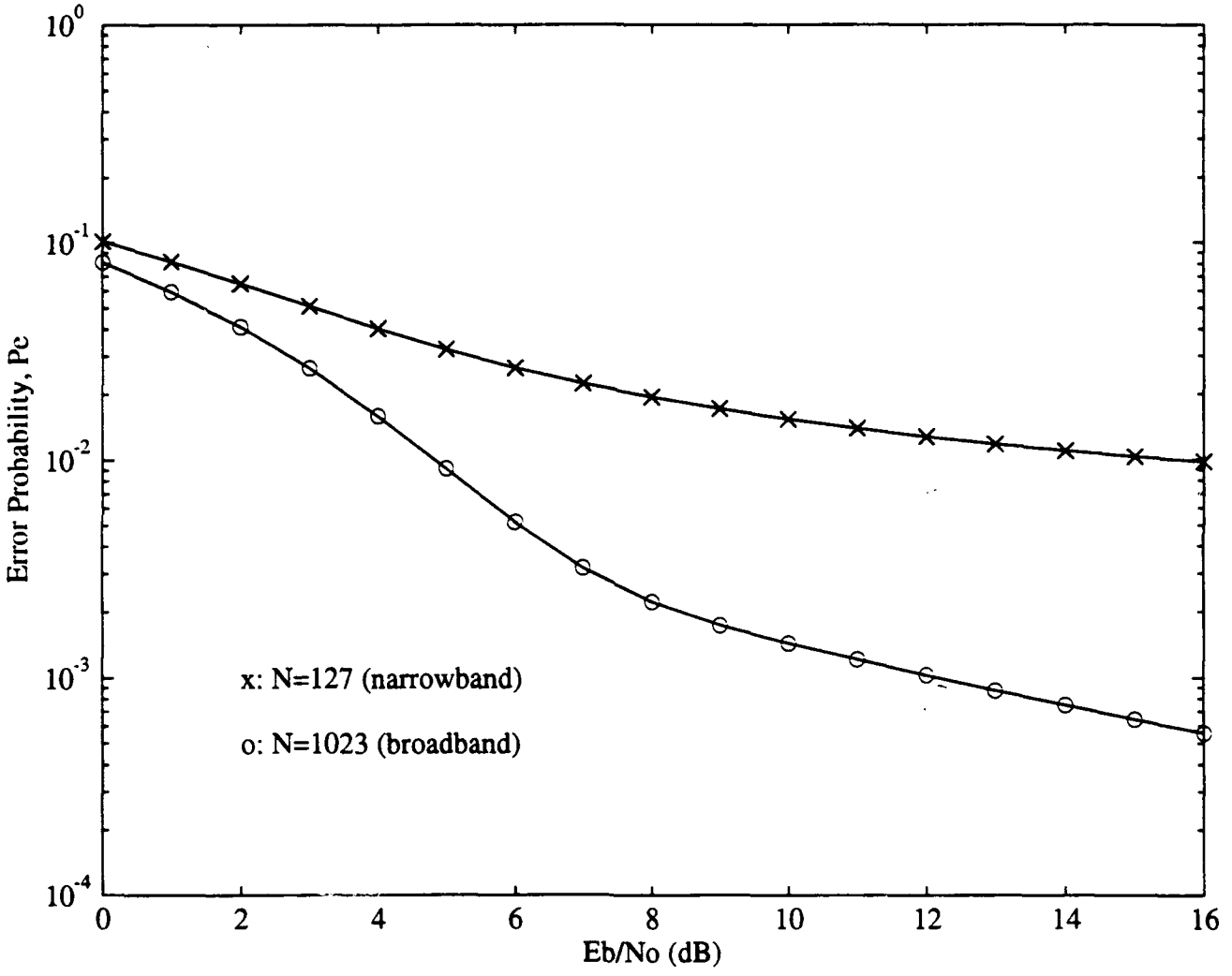

Figure 4: Probability of error for a particular multipath environment ($L = 12$ total paths, $\gamma_0^2 = 0$).

As shown by Figure 4, while the probabilities of error for both cases are fairly close at low E_b/N_0 values (0-3 dB), their relative difference does increase for higher E_b/N_0. Notice, though, that these systems perform rather poorly in comparison to previous situations; P_e lies above 10^{-4} even at $E_b/N_0 = 16$dB. This is due to several factors. First, the path delay region in which a portion of multipath rejection is unattainable (i.e., $\tau < T_c$) also has the greatest amount of relative power for each path ($\gamma^2 = 1$). As a result, this interference component receives the most emphasis of the four. Second, the high number of paths in total (12) should generally imply higher error probability, as proven from Figure 3.

Figure 5 compares three different systems for the length $N = 31$ signature sequence in which path delay is uniformly distributed in $[0, T_c]$, $\gamma_0^2 = 0$, and the sum of the multipath relative powers is constant for each system (i.e., $\sum_{n=1}^{L} \gamma_n^2 = L\gamma^2 = 0.2$). The total number of paths L increases from 2 to 100, as shown. The $L = 100$ curve coincides with the Gaussian approximation to the error probability, expressed in (26), which depends only on $\sum_{n=1}^{L} \gamma_n^2$.

The impact of the multipath interference is demonstrated by the significant difference between the $L = 2$ data and that of $L = 10$ and 100 for $E_b/N_0 > 11$ dB. More importantly, the figure shows that the performance of the characteristic-function method approaches that of the Gaussian model for high values of L. In the case of $L = 10$, the characteristic-function model appears Gaussian up to about $E_b/N_0 = 13$ dB, while for $L = 100$, the ab-

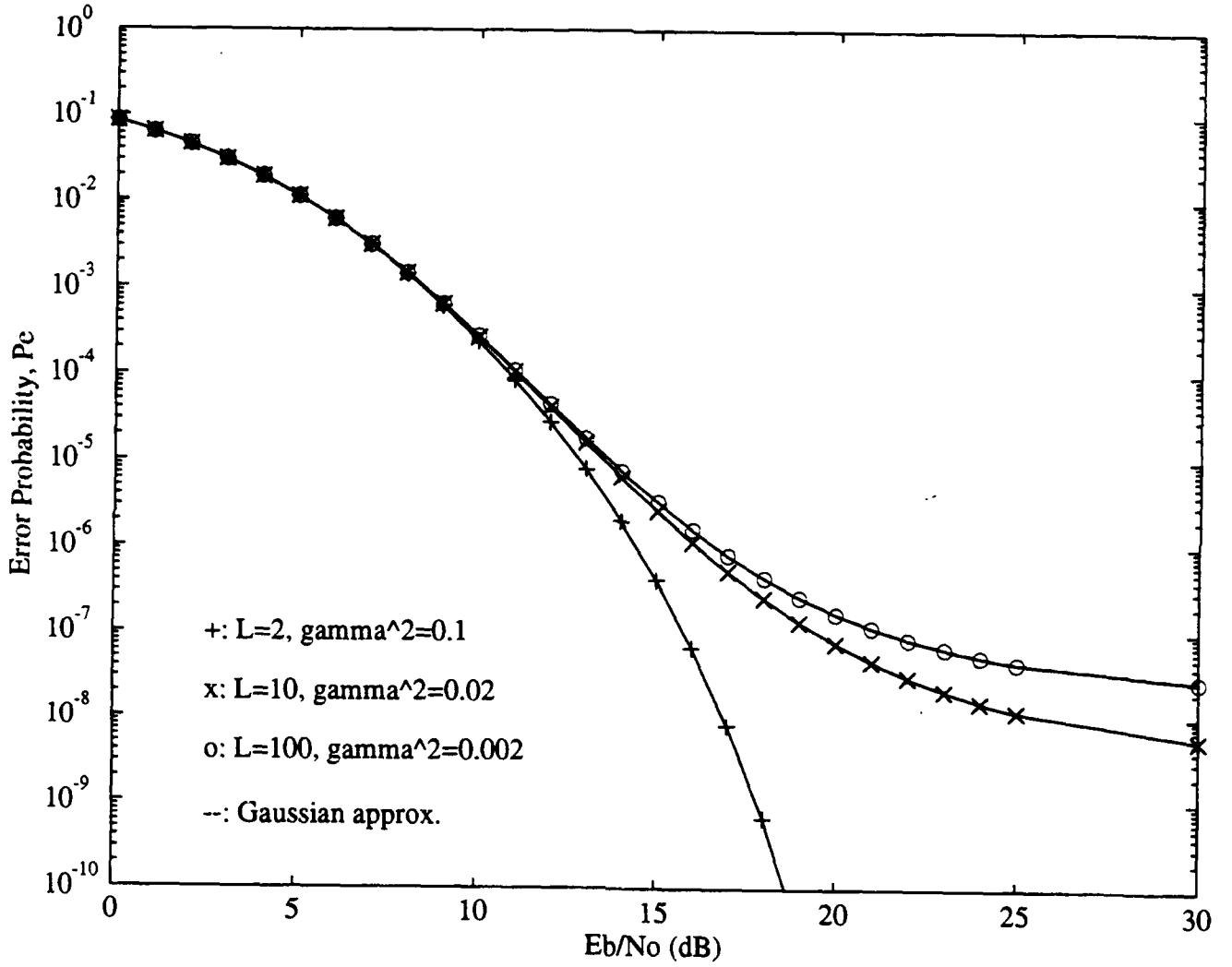

Figure 5: Probability of error for characteristic-function method approaching Gaussian approximation in performance ($N = 31, \tau \sim U[0, T_c], \gamma_0^2 = 0$).

solute difference in error probability is less than 2 x 10^{-8}. From the Central Limit Theorem, one would expect that for sufficiently high L the distribution of the multipath interference is indeed approximated by the Gaussian distribution.

The last two examples examine the performance of DS/SS systems with and without channel coding. In the first, rate-1/2 and 1/3 convolutional coding is applied to a system with $N = 31$ chips/data bit signature sequence and path delay $\tau \sim U[T_c, T - T_c]$; thus, the demodulating sequence has length $N = 62$ or 93 chips/ coded symbol, depending upon the chosen rate. Figure 6 compares the probability of error bounds (31,32) for the coded systems with the average error probabilities of uncoded systems with effectively similar chipping sequence lengths. That is, the rate-1/2 system is plotted against an uncoded one having sequence length $N = 63$ chips/data bit ($\mathcal{H} = 103$ and $\alpha_0 = 000010$ [4]) and $\tau \sim U[3T_c, 61T_c]$, while the counterpart for the rate-1/3 system has $N = 127$ chips/data bit and $\tau \sim U[5T_c, 123T_c]$, assuming the same data bit duration T of the original system. Both cases of soft and hard decisions are included, using (31)-(32). For soft decisions, a large number (>100) of quantization levels was chosen. The figure also shows the error probability for the system prior to any channel coding as a matter of reference. Comparisons of coded and uncoded systems is somewhat biased because the performance of the coded system is based on an upper bound, while the uncoded system is based on an exact calculation.

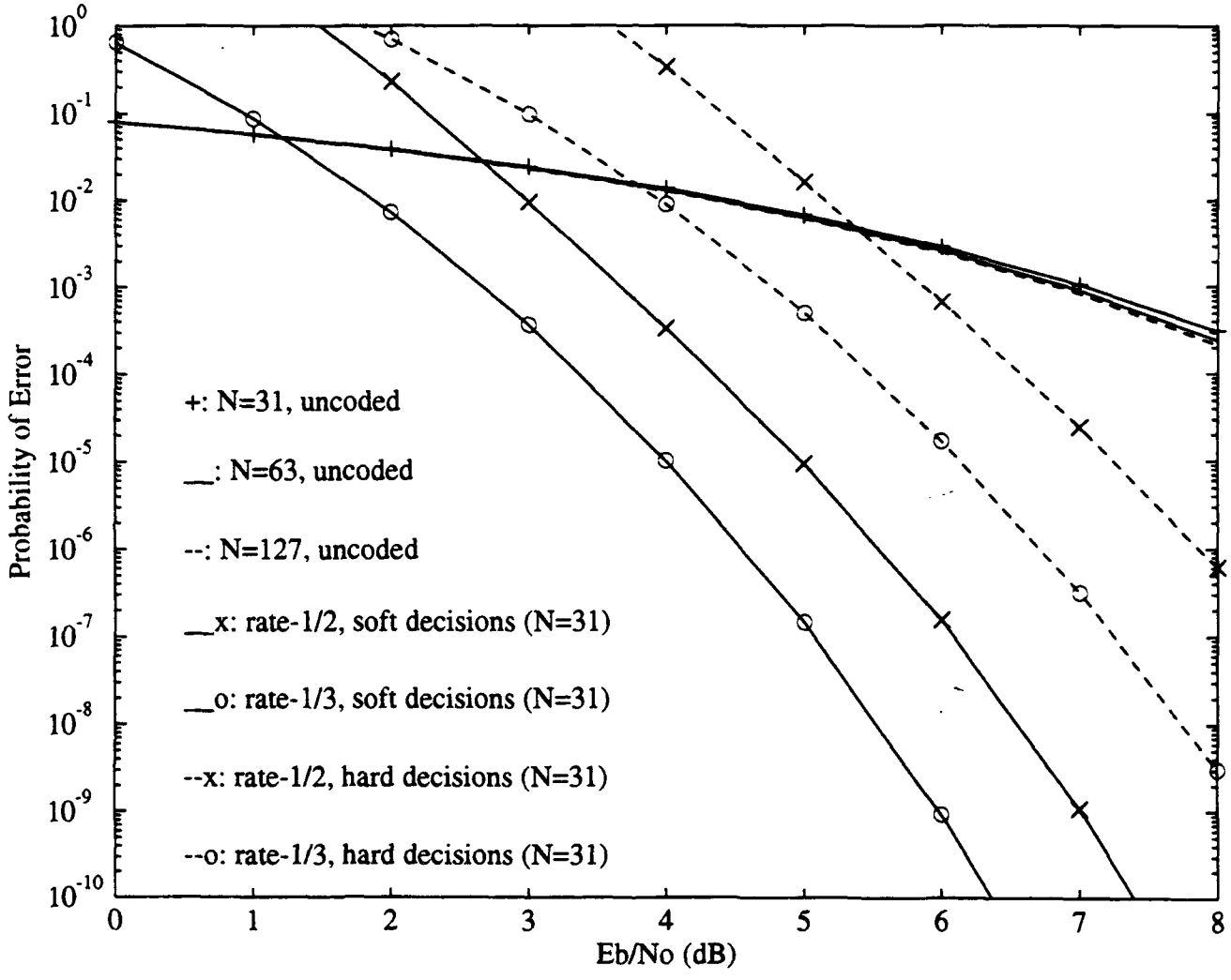

Figure 6: Probability of error for DS/SS systems, with and without channel coding ($L = 5, \gamma^2 = 0.4, \gamma_0^2 = 0$).

As expected, the coded systems achieve lower error probabilities for high E_b/N_0 than those of the comparison models. However, at E_b/N_0 less than about 5.5 dB, the rate-1/2 coded system with hard decisions starts to perform worse. When E_b/N_0 is as low as about 1.2 dB, even soft decisions with the rate-1/3 coded system fail to perform effectively. This is due to the fact that at sufficiently low input signal-to-noise ratios, channel coding exploits the weak energy of the data signal and introduces further errors to the system. As a result, it is not uncommon to even find error probabilities greater than one (e.g., rate-1/2 coding (hard decision) at $E_b/N_0 = 0$ dB). For the most part, the systems with soft decisions perform about 3 dB better than hard decision schemes.

Finally, the channel coding schemes above are applied to the fourth example situation in which there is a particular multipath environment for each system. Figures 7 and 8 show the same type of probability of error data as in the previous example for the narrowband and broadband spread-spectrum systems, respectively.

For the narrowband case ($N = 127$), an uncoded system with chipping sequence length $N = 255$($\mathcal{H} = 455$ and $\alpha_0 = 01101111$ [4]) is compared with a rate-1/2 coded system ($N = 254$ chips/information bit). Coding with soft decisions perform better after $E_b/N_0 = 3.8$ dB, while hard decisions produce lower error probability only after $E_b/N_0 = 7.3$ dB. The rate-1/3 coded systems ($N = 381$ chips/information bit) are analyzed against an uncoded

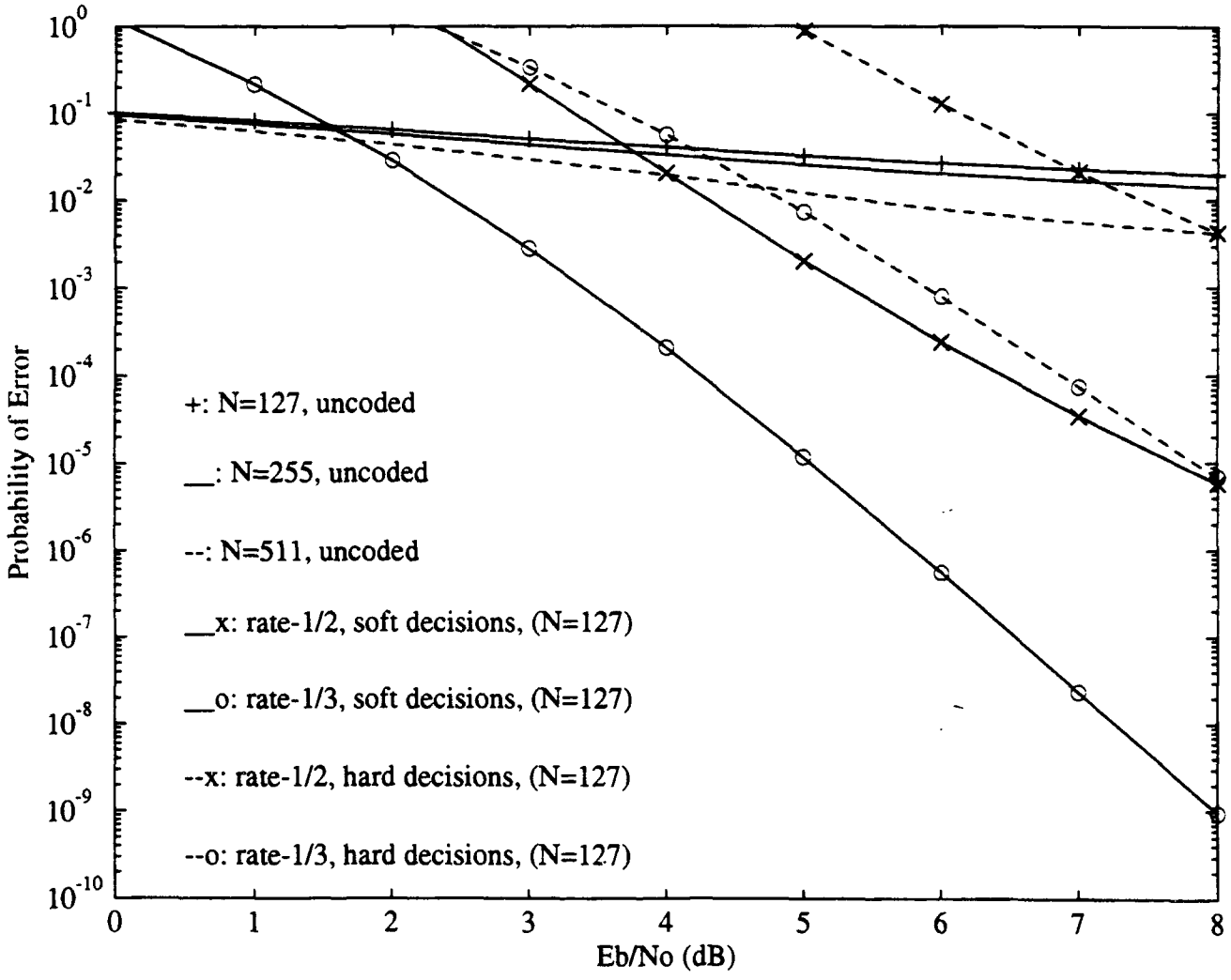

Figure 7: Probability of error for narrowband system and particular multipath environment, with and without channel coding ($L = 12$ total paths, $\gamma_0^2 = 0$).

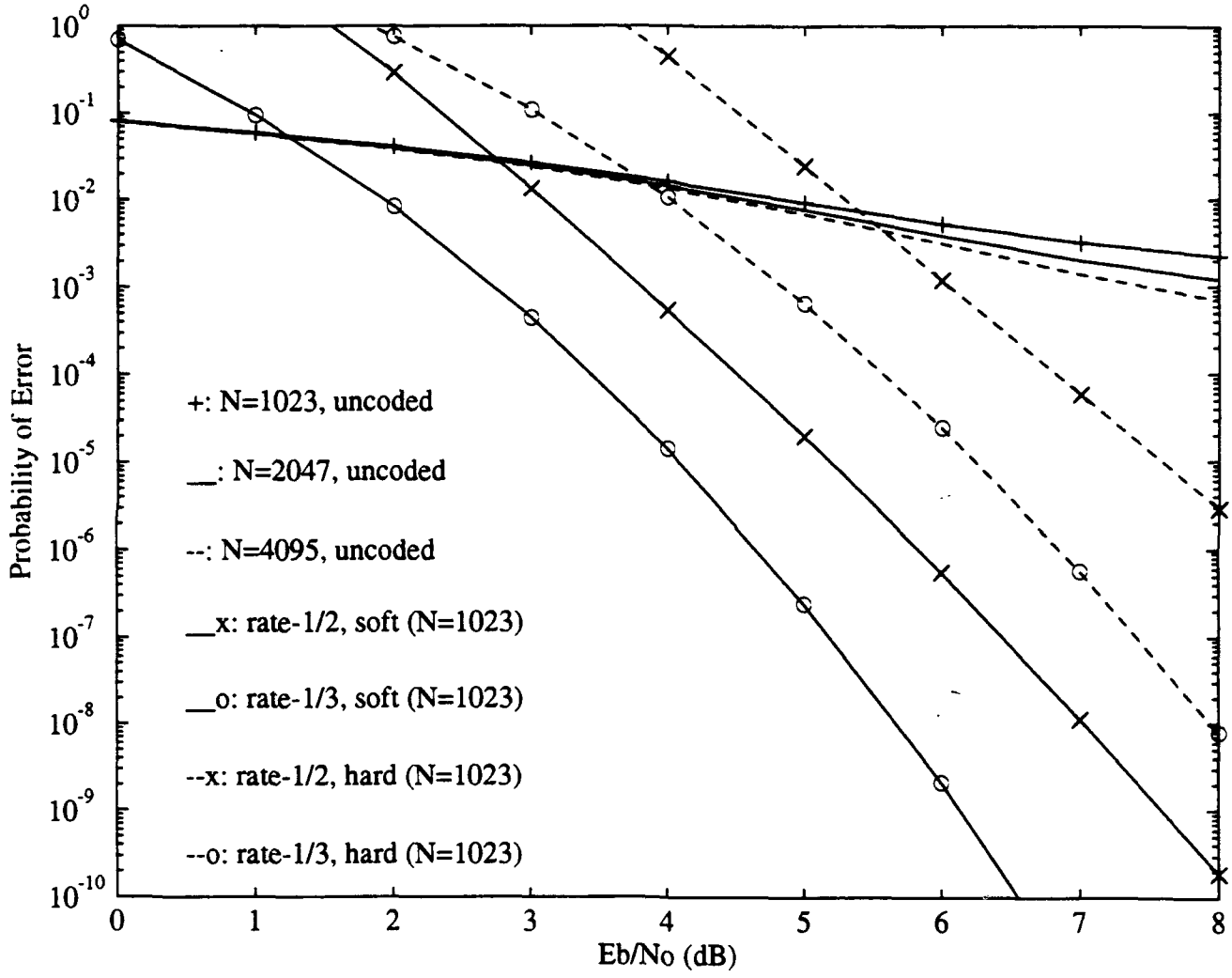

Figure 8: Probability of error for broadband system and particular multipath environment, with and without channel coding ($L = 12$ total paths, $\gamma_0^2 = 0$).

system with signature sequence $N = 511(\mathcal{H} = 1041$ and $\alpha_0 = 010101001$ [5]). Here, for $E_b/N_0 > 1.7$ dB, the soft-decision coding outperforms the uncoded system, while hard decisions take effect only after $E_b/N_0 = 4.7$ dB. The threshold distinguishing the effectiveness of soft decisions over hard decisions is at $E_b/N_0 = 2.4$ dB, prior to which the rate-1/3, hard-decision code does better than that with rate-1/2 soft decisions.

For the broadband case ($N = 1023$), the rate-1/2 coded system ($N = 2046$ chips/information bit) is compared with an uncoded system with chipping sequence length $N = 2047(\mathcal{H} = 5001$ and $\alpha_0 = 11000001000$ [5]). At $E_b/N_0 = 2.8$ dB, soft decisions begin to produce lower error probability, while the same is true for hard decisions at $E_b/N_0 > 5.5$ dB. The rate-1/3 coded system has bandwidth comparable to an uncoded system with $N = 4095(\mathcal{H} = 14501$ and $\alpha_0 = 101111000001)$. In this case, for $E_b/N_0 > 1.2$ dB, the coded system with soft decisions performs better than the uncoded comparison, while hard decisions do not take effect until after $E_b/N_0 = 3.9$ dB. For this particular system, the rate-1/3 code with hard decisions is more effective than the rate-1/2 code with soft decisions for $E_b/N_0 < 1.1$ dB.

6. Conclusions

From Figure 1, it is clear that the DS/SS system is only effective at rejecting multipath when the path delays are at least one chip period. One method of reducing the average probability of error is to increase the processing gain N. However, this comes at the expense of bandwidth and transmitter complexity (i.e., more shift registers required for signature sequence generation). When more delayed paths are added to the system, the multipath interference increases and system performance degrades rapidly. For a sufficiently high number of paths, the performance obtained via the characteristic-function method approaches that of the Gaussian approximation, as expected from the Central Limit Theorem.

The DS/SS system is significantly enhanced with the application of channel coding. In fact, according to Figure 6, the probability of error drops to 10^{-10} at about $E_b/N_0 = 6.3$ dB for a system with rate-1/3 convolutional coding and soft decisions applied. For the spread-spectrum systems with a particular multipath environment, there is a significant difference between the narrowband and broadband cases at low error probability (high E_b/N_0). However, for relatively higher probability of error (low E_b/N_0), the broadband system provides a 1-2 dB improvement over the narrowband counterpart.

7. References

[1] E. A. Geraniotis and M. B. Pursley, "Performance of Coherent Direct-Sequence Spread-Spectrum Communications Over Specular Multipath Fading Channels," *IEEE Transactions On Communications,* Vol. COM-33, pp. 502-508, June 1985.

[2] E. A. Geraniotis and M. B. Pursley, "Error Probability For Direct-Sequence Spread-Spectrum Multiple-Access Communications–Part II: Approximations," *IEEE Transactions On Communications,* Vol. COM-30, pp. 985-995, May 1982.

[3] M. B. Pursley, "Effects of Specular Multipath Fading on Spread-Spectrum Communications," in *New Concepts in Multi-User Communications* (NATO Advanced Study Institute–Series E), J. K. Skwirzynski, Ed. Alphen van den Rijn, The Netherlands: Sijthoff & Noordhoff, 1981, pp. 481-505.

[4] M. B. Pursley and H. F. A. Roefs, "Numerical Evaluation of Correlation Parameters For Optimal Phases of Binary Shift-Register Sequences," *IEEE Transactions On Communications,* Vol. COM-27, pp. 1597-1604, Oct. 1979.

[5] R. Skaug and J. F. Hjelstad, *Spread Spectrum In Communication,* Peter Peregrinus Ltd., London, UK, 1985, pp. 68-77.

[6] Jean Conan, "The Weight Spectra of Some Short Low-Rate Convolutional Codes," *IEEE Transactions On Communications*, Vol. COM-32, pp. 1050-1053, Sept. 1984.

Appendix A

Characteristic-Function Approach To Probability of Error

In this appendix, for purposes of completeness, we derive the expression in [1] for the average probability of error, given in terms of the characteristic functions of the multipath interference and noise. From (14) of the text, the error probability is expressed as

$$\bar{P}_e = \frac{1}{2} - \frac{1}{2}P(-1 < \eta + I \leq 1). \tag{33}$$

Letting $G = \eta + I$, and denoting the probability density of G by $f_G(g)$, (33) becomes

$$\bar{P}_e = \frac{1}{2} - \frac{1}{2}\int_{-1}^{1} f_G(g)dg. \tag{34}$$

Since the random variables η and I are mutually independent and have symmetric distributions, their characteristic functions, as well as that of their sum, must be real and even. Denoting the characteristic functions of η, I, and $\eta + I$ by ϕ_η, ϕ_I, and ϕ, respectively, $f_G(g)$ is given by

$$\begin{aligned} f_G(g) &= \frac{1}{2\pi}\int_{-\infty}^{\infty} e^{-jug}\phi(u)du \\ &= \frac{1}{\pi}\int_{0}^{\infty} \phi(u)\cos(gu)du \end{aligned}$$

since $f_G(g)$ must also be real-valued. Substituting into (34),

$$\bar{P}_e = \frac{1}{2} - \frac{1}{2}\int_{-1}^{1}\frac{1}{\pi}\int_{0}^{\infty} \phi(u)\cos(gu)dudg$$

$$= \frac{1}{2} - \frac{1}{\pi}\int_0^\infty \int_0^1 \phi(u)\cos(gu)dgdu$$
$$= \frac{1}{2} - \frac{1}{\pi}\int_0^\infty \phi(u)u^{-1}\sin(u)du.$$

To avoid subtracting very large numbers relative to their difference, one may replace $\phi(u) = \phi_\eta\phi_I$ with $\phi_\eta - \phi_\eta[1-\phi_I]$. Thus,

$$\bar{P}_e = \frac{1}{2} - \frac{1}{\pi}\int_0^\infty u^{-1}\sin(u)\phi_\eta(u)du + \frac{1}{\pi}\int_0^\infty u^{-1}\sin(u)\phi_\eta(u)[1-\phi_I(u)]du. \quad (35)$$

In the absence of interference (i.e., $I = 0$), $\phi_I = 1$ and error is due only to the presence of Gaussian noise. Denoting this noise error probability by P_η, (34) becomes

$$\bar{P}_e = P_\eta + \pi^{-1}\int_0^\infty u^{-1}\sin(u)\phi_\eta(u)[1-\phi_I(u)]du. \quad (36)$$

Since η is Gaussian, P_η is given by $Q(\sigma^{-1})$, where σ^2 is defined as the variance of η. The result is (15) of the text.

Appendix B

Computer Programs For Characteristic-Function Method

The following programs provide simulations for the average probability of error (15), the Gaussian approximation (26), and error bounds for coding (31,32). The computer code is written in MATLAB version 4.0 and all integrations are approximated applying Simpson's method.

The first program, **PROBERROR.m**, computes the average probability of error for both the characteristic-function method and the Gaussian approximation. The user is able to select the desired signature sequence from a menu; the program assumes existing data files containing the sequence itself and all the appropriate autocorrelation functions. The user may also create one or more multipath environments, each with a desired range for the path delay. The following function files are called within the main program:

SIMP.m – A Simpson's approximation to the $\tilde{\phi}_0$ integral.

PHI.m – Computes $\tilde{\phi}$; calls function file FF.m which provides Simpson's method for function $f(v; l, h)$.

The second program, **PROBMASS.m**, first determines the probability mass function for the quantized receiver output (29). This is then used to compute the distance parameter D (30), which is applied in approximating upper probability bounds for channel coding purposes; the program considers

convolutional coding with rates 1/2 and 1/3. The pmf data is calculated from the same two function files of the previous program.

```
% PROBERROR.m
%
% A program to compute the average probability of error of a DS/SS system with
% multipath fading and BPSK modulation, using both the characteristic-function
% method and the Gaussian approximation.  Path delay is uniform from one
% multiple of Tc to another for a given number of paths within each multipath
% environment.  User selects desired chipping sequence from a menu.
%
% Input: gamma0^2 (assumed constant); for each path delay situation -- number of
%        paths L, gamma^2, uniform range for path delay; Eb/No, upper limit and
%        number of points of integration for Simpson's method.
%
% Output: for each Eb/No, average probability of error for both characteristic-
%         function method and Gaussian approximation.
%

clear; format long e;
k = menu('Choose sequence length','N=31','N=63','N=127','N=255','N=511',...
         'N=1023','N=2047','N=4095');
if k == 1,
        load code_31     % each signature sequence file contains the actual
                         % sequence (code) and all autocorrelation functions:
elseif k == 2,           % aperiodic: R          periodic(even): theta
        load code_63     % odd: thetahat
elseif k == 3,
        load code_127
elseif k == 4,
        load code_255
elseif k == 5,
        load code_511
elseif k == 6,
        load code_1023
elseif k == 7,
        load code_2047
else
        load code_4095
end
disp('Enter the requested data:')
gamma0sq = input('gamma_0-squared = '); % assumed to be constant for all
                                        % multipath environments.
gamma0 = sqrt(gamma0sq);
sit = input('How many different delay situations are there? ');
for j = 1:sit
        disp('situation #'); disp(j);
        L(j) = input('no. of paths L = ');
        gammasq(j) = input('gamma-squared = ');
        disp('Path delay tau ~ U[M1*Tc, M2*Tc]:')
        M1(j) = input('constant multiple M1 = ');
        M2(j) = input('constant multiple M2 = ');
        gamma(j) = sqrt(gammasq(j));
end;
N = length(code);        % length of sequence

data = input('How many Eb/No data values? ');
ssum1 = zeros(1,data); ssum2 = zeros(1,data);
for d = 1:data
        EbN0_dB(d) = input('Enter Eb/N0 value (dB):');
        b = input('upper-limit of integration = ');
```

```
        n = input('no. of pts. (must be even) for integration = ');
        h = b/n; EbN0(d) = 10^(EbN0_dB(d)/10);
        sigmasq(d) = 1/(2*EbN0(d)); sigmainv(d) = 1/sqrt(sigmasq(d));

        Q(d) = Qfunct(sigmainv(d));      % compute the Q-function of sigma-
                                         % inverse.

        i = [0:n];       % Simpson's method starts here, done using vector form.
        u = 1E-100 + i*h;
        phi_eta= exp(-(u.^2) * (sigmasq(d))/2);
        phi_tilde_0 = 2/pi * simp(gamma0*u, pi/2, 20);  % SIMP.m is a function
                                                        % which performs
                                                        % Simpson's method for
                                                        % phi_tilde_0.

        phi_tilde = phi(gamma'*u,L,M1,M2,N,theta,thetahat);  % see separate
                                                             % listing for
                                                             % function PHI.m.
        phi_I = phi_tilde_0 .* phi_tilde;
        g = ones(1,n+1)./u .* sin(u) .* (1-phi_I) .* phi_eta;

        coeff = 2 * (rem(i,2)+1);        % coefficients for Simpson's summation.
        coeff(1) = 1; coeff(n+1) = 1;
        ssum(d) = sum(coeff .* g);
        simpson(d) = h/3 * ssum(d);
        proberr(d) = Q(d) + 1/pi * simpson(d);  % this is eq. (15) of text.

% This section computes the Gaussian approximation
        sum2 = 0;
        for j = 1:sit
                sum1 = 0;
                for lg = M1(j):M2(j)-1
                    sum1 = sum1 + R(2*N+1-lg)*R(2*N-lg) + R(N+1+lg)*R(N+2+lg)...
                                + R(2*N+1-lg)^2 + R(2*N-lg)^2 + R(N+1+lg)^2 + ...
                                  R(N+2+lg)^2;
                end
                sum2 = sum2 + 1/6 * L(j)*gammasq(j)/(N^2*(M2(j)-M1(j))) * sum1;
        end
        SNR_0 = 1 / sqrt(sigmasq(d) + sum2);

        ng = 500;        % choose 500 points for Simpson's method integration.

        ig = [0:ng]; hg = pi/ng;   % may use pi as an upper limit since function
                                   % for integration is even
        thetag = ig*hg;
        g = Qfunct(SNR_0*(1 + gamma0*cos(thetag)));
        coeffg = 2 * (rem(ig,2)+1);
        coeffg(1) = 1; coeffg(ng+1) = 1;
        ssumg(d) = sum(coeffg .* g);
        simpsong(d) = hg/3 * ssumg(d);
        proberrg(d) = 1/pi * simpsong(d);   % 1/pi factor instead of 1/(2pi)
                                            % since integrating only to pi; this
                                            % is eq. (26).

        disp('ave. prob. of error for char-funct method = '); disp(proberr(d))
        disp('Gaussian approximation to prob. of error = '); disp(proberrg(d))
end
```

```
function simpson = simp(const,b,n)

% SIMP        Simpson's rule for phi_tilde_0 characteristic function.
%
%             Input: gamma_0*u (const), upper-limit (b) and number of points for
%                    integration (n).
%
%             Output: Simpson's approximation to the integral.

h = b/n; ssum = 0;
i = [0:n];
theta = i*h;
g = cos(const' * cos(theta));    % function for inegration.

coeff = 2 * (rem(i,2)+1);        % coefficients for approximation.
coeff(1) = 1; coeff(n+1) = 1;
ssum = coeff * g';
simpson = h/3 * ssum;    % Simpson's approximation
```

```
function out = phi(var,L,M1,M2,N,theta,thetahat)

% PHI   Characteristic function phi_tilde(u).  Function f for theta and thetahat
%       is called by FF.m.
%
%       Input: variable (var), no. of reflected paths (L), constant multiples of
%              Tc (M1,M2), length of signature sequence (N), and autocorrelation
%              vectors theta and thetahat.
%
%       Output: the value of the characteristic function.

s = length(L);  % number of multipath environments.

prod1 = 1; prod2 = 1;
for j = 1:s
        ssum1 = 0; ssum2 = 0;
        for l = M1(j):M2(j)-1
                f = ff(var(j,:),l,theta,N);        % compute f for theta and
                                                   % thetahat
                f_hat = ff(var(j,:),l,thetahat,N);

                ssum1 = ssum1 + f;
                ssum2 = ssum2 + f_hat;
        end
        out1 = (1/(M2(j)-M1(j)) * ssum1) .^ L(j);
        out2 = (1/(M2(j)-M1(j)) * ssum2) .^ L(j);
        prod1 = prod1 .* out1;
        prod2 = prod2 .* out2;
end
out = 0.5 * (prod1 + prod2);    % this corresponds to phi_tilde(u).
```

```
function f = ff(v,k,t,N)

% FF    Function f for vectors theta and thetahat.  Considers zeroeth index for
%       autocorrelation vectors.  Input is real variable (v), index (k),
%       autocorrelation vector (t), and length of code sequence (N).  Output is
%       Simpson's formula approximation.

b = pi/2; n = 20;       % only 20 points are necessary for good approximation.
h = b/n;
i = [0:n]; l = k+1;
theta = i*h;
g1 = sinc(v'*(t(l+1)-t(l))*cos(theta)/(2*pi*N));  % SINC.m simply performs the
                                                  % sinc function for given
                                                  % variable.
g2 = cos(v'*(t(l+1)+t(l))*cos(theta)/(2*N));
g = g1 .* g2;
coeff = 2 * (rem(i,2)+1);
coeff(1) = 1; coeff(n+1) = 1;
ssum = coeff * g';
simpson = h/3 * ssum; f = 2/pi * simpson;       % this is the function f.
```

```
% PROBMASS.m
%
% A program to compute the probability mass function of Z, P(a<Z<b|b0), of a
% multipath DS/SS system with BPSK modulation. Path delay is uniform from one
% multiple of Tc to another, for a given number of multipath environments.  User
% selects desired chipping sequence from a menu.  Here, gamma0-squared(gamma0sq)
% is assumed to be zero, but may be reset to constant for all delay situations.
% The pmf is used, in turn, to determine the Hamming D-parameter and apply
% toward computing the probability error bounds for specific channel coding.
%
% Input: for each delay invironment -- number of paths (L), gamma-squared
%                                      (gammasq), Tc multiples (M1,M2);
%        total number of ranges for receiver output Z, epsilon increment, Eb/No,
%        upper limit and no. of points for integration using Simpson's method.
%
% Output: probability error bounds for rate-1/2 and 1/3 convolutional codes

clear; format long e;
k = menu('Choose sequence length','N=31','N=127','N=1023')
if k == 1,
        load code_31
elseif k == 2,
        load code_127
else
        load code_1023
end
disp('Enter the requested data:')

sit = input('How many different delay situations are there? ');

for j = 1:sit   % same data requested as in PROBERROR.m

        disp('situation #'); disp(j);
        L(j) = input('no. of paths L = ');
        gammasq(j) = input('gamma-squared = ');

        disp('Path delay tau ~ U[M1*Tc, M2*Tc]:')
        M1(j) = input('constant multiple M1 = ');
        M2(j) = input('constant multiple M2 = ');

        gamma0sq=0;  % assume gamma0-squared is zero throughout.

        gamma(j) = sqrt(gammasq(j)); gamma0 = sqrt(gamma0sq);
end;
N = length(code);
num = input('How many Eb/No values?');
for g = 1:num
        EbN0_dB(g) = input('Enter Eb/N0 (dB):');
        eps = input('Enter increment epsilon:');   % increment used in mapping
                                                   % out the discrete Z values.

        data = input('How many total ranges for Z (even)? ');

        p = [-data/2:data/2];   % split the desired ranges into positive and
                                % negative regions.

        Eb(g) = 10^(EbN0_dB(g)/10); N0(g) = 1;  % the energy per information bit
                                                % Eb, is needed specifically.
```

```
E2(g) = Eb(g)/2; E3(g) = Eb(g)/3;        % this is the energy per coded
                                         % symbol for rates-1/2 and 1/3
                                         % codes.

EN02(g) = (Eb(g)/N0(g))/2; EN03(g) = (Eb(g)/N0(g))/3;
bb = input('upper-limit of integration = ');
n = input('no. of pts. (must be even) for integration = ');
h = bb/n;
sigmasq2(g) = 1/(2*EN02(g)); sigmasq3(g) = 1/(2*EN03(g));
sigmainv2(g) = 1/sqrt(sigmasq2(g)); sigmainv3(g) = 1/sqrt(sigmasq3(g));

d2 = eps*p*sqrt(E2(g)); d3 = eps*p*sqrt(E3(g));  % these are the actual
                                                 % values for Z.

a2 = d2(1:data); a3 = d3(1:data);        % a and b the range limits for
b2 = d2(2:data+1); b3 = d3(2:data+1);    % the Z values. Throughout, a
                                         % 2-suffix refers to a variable
                                         % for rate-1/2 code, while a
                                         % 3-suffix refers to that for
                                         % rate-1/3 code.
i = [0:n];
u = 1E-100 + i*h;
uinv = ones(1,n+1)./u; uinvd = uinv;
phi_eta2 = exp(-(u.^2) * sigmasq2(g)/2);
phi_eta3 = exp(-(u.^2) * sigmasq3(g)/2);
phi_etad2 = phi_eta2; phi_etad3 = phi_eta3;
phi_tilde_0 = 2/pi * simp(gamma0*u, pi/2, 20);
phi_tilde = phi(gamma'*u,L,M1,M2,N,theta,thetahat);
phi_I = phi_tilde_0 .* phi_tilde; phi_Id = phi_I;

for m = 1:data-1          % generates data-length column vectors for
                          % u-inverse, phi_eta, and phi_I.

        uinvd = [uinvd; uinv];
        phi_etad2 = [phi_etad2; phi_eta2];
        phi_etad3 = [phi_etad3; phi_eta3];
        phi_Id = [phi_Id; phi_I];
end

% computes functions for Simpson's method, considering both b0=+1 (pos)
% and b0=-1 (neg).

sindiff2pos = sin((b2'/sqrt(E2(g))-1)*u) - sin((a2'/sqrt(E2(g))-1)*u);
sindiff3pos = sin((b3'/sqrt(E3(g))-1)*u) - sin((a3'/sqrt(E3(g))-1)*u);
sindiff2neg = sin((b2'/sqrt(E2(g))+1)*u) - sin((a2'/sqrt(E2(g))+1)*u);
sindiff3neg = sin((b3'/sqrt(E3(g))+1)*u) - sin((a3'/sqrt(E3(g))+1)*u);
g12pos = uinvd .* sindiff2pos .* phi_etad2;
g13pos = uinvd .* sindiff3pos .* phi_etad3;
g22pos = uinvd .* sindiff2pos .* (1-phi_Id) .* phi_etad2;
g23pos = uinvd .* sindiff3pos .* (1-phi_Id) .* phi_etad3;
g12neg = uinvd .* sindiff2neg .* phi_etad2;
g13neg = uinvd .* sindiff3neg .* phi_etad3;
g22neg = uinvd .* sindiff2neg .* (1-phi_Id) .* phi_etad2;
g23neg = uinvd .* sindiff3neg .* (1-phi_Id) .* phi_etad3;
coeff = 2 * (rem(i,2)+1);
coeff(1) = 1; coeff(n+1) = 1;
ssum12pos = coeff * g12pos'; ssum13pos = coeff * g13pos';
ssum22pos = coeff * g22pos'; ssum23pos = coeff * g23pos';
```

```
ssum12neg = coeff * g12neg'; ssum13neg = coeff * g13neg';
ssum22neg = coeff * g22neg'; ssum23neg = coeff * g23neg';
simpson12pos = h/3 * ssum12pos; simpson13pos = h/3 * ssum13pos;
simpson22pos = h/3 * ssum22pos; simpson23pos = h/3 * ssum23pos;
simpson12neg = h/3 * ssum12neg; simpson13neg = h/3 * ssum13neg;
simpson22neg = h/3 * ssum22neg; simpson23neg = h/3 * ssum23neg;
probmass2pos = 1/pi*simpson12pos - 1/pi*simpson22pos;
probmass3pos = 1/pi*simpson13pos - 1/pi*simpson23pos;

% the probability mass function is assumed to be zero for the final
% value of Z and thereafter; probmass... is eq. (29) for a and b values
% above.

probmass2pos(data+1) = 0; probmass3pos(data+1) = 0;
probmass2neg = 1/pi*simpson12neg - 1/pi*simpson22neg;
probmass3neg = 1/pi*simpson13neg - 1/pi*simpson23neg;
probmass2neg(data+1) = 0; probmass3neg(data+1) = 0;

% this shows how close the sum of the pmfs is to 1.

disp('summation error (1/2) pos = '); disp(1-sum(probmass2pos));
disp('summation error (1/3) pos = '); disp(1-sum(probmass3pos));
disp('summation error (1/2) neg = '); disp(1-sum(probmass2neg));
disp('summation error (1/3) neg = '); disp(1-sum(probmass3neg));

stairs(d2,probmass2pos); pause    % plot the pmf in stairs mode.
stairs(d2,probmass2neg); pause
stairs(d3,probmass3pos); pause
stairs(d3,probmass3neg);
D2(g) = sum(sqrt(probmass2pos .* probmass2neg));   % this is the
                                                   % D-parameter
D3(g) = sum(sqrt(probmass3pos .* probmass3neg));   % eq. (30).

% the following formulas are approximations to the probability error
% bounds for rate-1/2 and rate-1/3 convolutional codes -- eqs. (31,32).

bound2(g) = 36*D2(g)^10 + 211*D2(g)^12 + 1404*D2(g)^14 ...
          + 11633*D2(g)^16 + 77433*D2(g)^18 + 502690*D2(g)^20;

bound3(g) = 11*D3(g)^18 + 32*D3(g)^20 + 195*D3(g)^22 + 564*D3(g)^24 ...
          + 1473*D3(g)^26;
disp('error bound for rate-1/2 code = '); disp(bound2(g));
disp('error bound for rate-1/3 code = '); disp(bound3(g));
```

nd